Technical Sciences
Academy of Romania
www.jesi.astr.ro

Journal of Engineering Sciences and Innovation
Volume 10, Issue 4 / 2025, pp. 431 - 444
http://doi.org/10.56958/jesi.2025.10.4.431

C. Chemical Engineering, Materials Science and Engineering

Received ***5 July 2025*** *Accepted* ***10 December 2025***
Received in revised form ***31 October 2025***

Anodic oxidation of sulfite ions on AISI 304 stainless steel in alkaline medium

MIRCEA-LAURENȚIU DAN[1], NATALIA RUDENKO[1], NICOLAE VASZILCSIN[1,2], GEORGE DIMA[1], GABRIELA-ALINA DUMITREL[1*]

[1]University Politehnica Timișoara, 2 Piața Victoriei, Timișoara, România
[2]Technical Sciences Academy of Romania, 26 Bd. Dacia, sector 1, 010413, Bucharest

Abstract. Research focused on the electrochemical oxidation of sulfites continues to be relevant, on the one hand, in order to minimizing their environmental effect, and on the other hand, to exploiting their energy potential in fuel cells. Generally, the anodic oxidation of sulfite has been studied on platinum, gold, and graphite. Since platinum and gold are expensive, and graphite is consumed during the anodic reaction, our research focused on the use of an austenitic stainless steel (AISI 304). Cyclic voltammograms recorded on AISI 304 steel in 1 mol L^{-1} NaOH solution, at different sulfite concentrations, revealed characteristic peaks of sulfite ion oxidation. At higher anodic potentials, oxygen evolution was observed. Kinetic parameters (exchange current density i_o and anodic transfer coefficient α) were determined using the potentiodynamic polarization method. The obtained values were comparable to those reported in the literature for noble metals, indicating the potential of AISI 304 steel as an anode material in sulfite/air fuel cells. The results from potentiodynamic polarization were confirmed by electrochemical impedance spectroscopy.

Keywords: sulfite/air fuel cells, sulfite oxidation, electrochemical characterization.

1. Introduction

Sulfites are by-products generated in several industrial processes, such as the combustion of fossil fuels, particularly solid fuels. To reduce the costs associated with sulfite oxidation, their use as anodic depolarizers in sulfite/air fuel cells has been proposed. In such fuel cells, sulfite is oxidized to sulfate at the anode (1), while oxygen reduction occurs at the cathode (2).

*Correspondence address: alina.dumitrel@upt.ro

$$SO_3^{2-} + 2HO^- \rightarrow SO_4^{2-} + H_2O + 2e^- \quad (1)$$

$$O_2 + 2H_2O + 4e^- \rightarrow 4HO^- \quad (2)$$

When assessing the electromotive force of a sulfite/air fuel cell, Latimer diagrams are used [1]. For example, in alkaline medium, at pH = 14, the standard potential of the sulfite/sulfate redox couple is −0.936 V, whereas the standard potential of the O_2/HO^- couple is +0.401 V [2]. Consequently, the standard electromotive force of a sulfite/ oxygen fuel cell will be 1.337 V.

Sulfite ions (SO_3^{2-}/HSO_3^-), mostly generated in industrial flue gas desulfurization, paper pulp extraction, or sulphur dioxide capture systems, represent an environmental hazard and a prospective avenue for energy conversion via electrocatalysis [3]. The anodic oxidation of sulfite to sulphate not only neutralises these chemicals but also offers the potential for their application in renewable electrochemical devices, such as sulfite/oxygen cells or electrolysis processes for hydrogen production [4].

Noble metals such as gold and platinum have excellent electrocatalytic activity for the oxidation of Na_2SO_3; nevertheless, their practical use is impeded by their elevated cost and the occurrence of sulphuric adsorption [5-7]. Consequently, recent research has focused on cost-effective alternative materials, such as lead oxide on platinum [11], graphite-gold composites [10], and nickel-based electrodes adorned with platinum nanoparticles[8,9]. Nonetheless, despite their superior corrosion resistance, durability, and cost-effectiveness, stainless steels - especially AISI 304 - have garnered minimal attention in the literature on the anodic oxidation of sulfite. The passive chromium oxide layer that develops on AISI 304 steel, composed of iron, chromium, and nickel, might influence electron transport during anodic processes in an alkaline medium [12]. Research on 304L indicates that, without significant enhancements to the untreated surface, the anodic coating gradually thickens and provides electrochemical stability in saline conditions [13].

Furthermore, anodic characterisation in a pH = 8 SO_4^{2-}/HCO_3^- medium indicates that the surface remains passive, exhibiting a continuous anodic current without significant peaks [14]. Moreover, specific investigations in sulphurous or sulfuritic environments indicate that the anodic oxidation of sulphites on SS304 is constrained by mass transfer control[15].

The $SO_2/HSO_3^-/SO_3^{2-}$ equilibrium diagram [16] demonstrates that SO_3^{2-} is the predominant species under alkaline conditions (pH > 9). The processes at this pH may vary from direct oxidation to radical-mediated oxidation, contingent upon the anode material. The kinetic behaviour of oxidation processes is directly affected by passive film development and alterations on non-noble surfaces such as stainless steel [17]. This study investigates the anodic oxidation of sulfite ions on AISI 304 stainless steel in an alkaline setting. The objectives encompass characterising the processes (direct/indirect, radicals, passivation effect) and evaluating the electrochemical performance and stability of sulfite to sulphate oxidation. The efficacy of AISI 304 as a cost-efficient and durable electrode for the electrochemical conversion of sulfites in industrial environmental applications was

validated by cyclic voltammetry, chronoamperometry, and surface analysis methods (optical microscopy).

2. Materials and methods

An undivided thermostatic cell was employed for the experimental phase, linked to an SP-150 Biological potentiostat for electrochemical studies, including cyclic voltammetry, linear voltammetry, chronoamperometry, and electrochemical impedance spectroscopy. The cell included three electrodes: an AISI 304 working electrode with an active surface area of 1 cm^2, two graphite counter electrodes, and an Ag/AgCl reference electrode, with all potentials measured relative to E = +0.197 V. For the preparation of the electrolyte solutions, NaOH ACS reagent with a purity of 97% and Na_2SO_3 with a purity of 98%, both manufactured by Sigma Aldrich, were utilized. The experimental measurements were conducted in a 1 mol L^{-1} NaOH (BS) solution, devoid of many amounts of sulfite, namely 10^{-3}, 10^{-2}, 10^{-1}, 0.5, and 1 mol L^{-1}. The cyclic voltammetry studies were conducted at polarization rates of 500, 50, and 5 mV s^{-1}, whereas linear voltammograms were recorded at a rate of 2 mV s^{-1} to achieve quasi-stationary conditions. Electrochemical impedance spectroscopy (EIS) studies were performed using the impedance module of SP-150, in the frequency range from 10 mHz to 100 kHz and AC voltage amplitude of 10 mV. For each spectrum, 60 points were collected, with a logarithmic distribution of 10 points per decade. The experimental EIS data were fitted to the electrical equivalent circuit by CNLS Levenberg-Marquardt procedure using Zview-Scribner Associates Inc. software. Sulphite oxidation efficiency has been determined by chronoamperometry and chronocoulometry methods.

3. Results and discussions

3.1. Cyclic voltammetry

Cyclic voltammograms (CV) were obtained on AISI 304 electrode in 1 mol L^{-1} NaOH, with and without various amounts of sodium sulfite (10^{-3}, 10^{-2}, 10^{-1}, 0.5, and 1 mol L^{-1}) to elucidate the redox processes at the electrode/electrolyte interface. To illustrate the effect of polarisation rate on electrochemical processes, tests were performed in potentiodynamic mode at scanning velocities of 500, 50, and 5 mV s^{-1} (Figure 1).

An oxidation peak between 0.4 and 0.8 V vs. Ag/AgCl is seen during anodising in the absence of SO_3^{2-} ions (curve 1), and this peak is associated with the generation of atomic oxygen adsorbed on the electrode surface. As the concentration of sodium sulfite increases, this peak diminishes in intensity, and at concentrations of 10^{-1} mol or greater, it entirely disappears. The oxidation process of sulfite on the electrode surface and the competitive adsorption of SO_3^{2-} ions on the active surface account for this behaviour.

$$SO_3^{2-} + H_2O \rightarrow SO_4^{2-} + 2H^+ + 2e^- \quad (3)$$

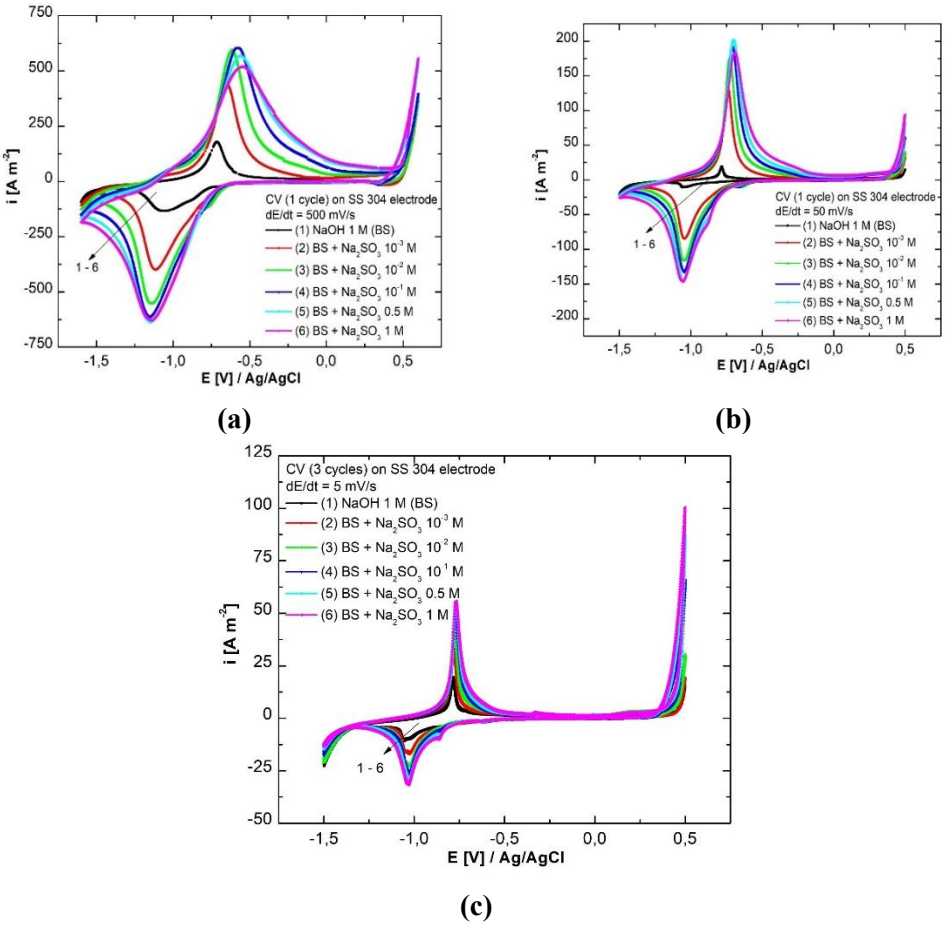

Fig. 1. Cyclic voltammograms recorded on an AISI 304 electrode at scan rates of (a) 500 mV s^{-1}, (b) 50 mV s^{-1}, and (c) 5 mV s^{-1} in solutions containing various concentrations of sulfite.

At higher anode polarisations, notably at 500 mV s^{-1}, direct oxidation of sulfite and oxidation facilitated by adsorbed oxygen occur concurrently (Figure 1a). The overlap of these processes considerably enhances the density of anode current in relation to the increased sulfite concentration. The primary processes in the anodic domain are sulfite oxidation and the oxygen evolution reaction (OER).

$$2H_2O \rightarrow O_2 + 4H^+ + 4e^- \quad (4)$$

The hydrogen evolution process (HER), characteristic of the alkaline environment, transpires on the cathode segment of voltammograms at potentials above −1.0 V.

$$2H_2O + 2e^- \rightarrow H_2 + 2OH^- \quad (5)$$

The redox currents are diminished at lower scan rates (50 mV s^{-1}, Figure 1b, and 5 mV s^{-1}, Figure 1c), although the structure of the curves more distinctly depicts the equilibrium between adsorption and charge transfer processes. At a scan rate of 5

mV s^{-1}, a clear distinction between the oxidation and reduction peaks is observed, signifying the significant influence of diffusion processes.
At higher quantities (≥ 0.1 mol L^{-1}), the oxidation of sulfite prevails in the anodic domain, competing with and perhaps inhibiting the generation of atomic oxygen on the SS304 electrode surface. These data confirm a hybrid process of direct and mediated oxidation, regulated by concentration and polarization rate.

3.2. Linear sweep voltammetry

The current density variation as a function of electrode potential in the anodic domain was acquired by linear voltammetry at a low scan rate. Figure 2 illustrates the curves recorded at 2 mV s^{-1} under alkaline conditions (1 mol L^{-1} NaOH) with different quantities of SO_3^{2-} ions (spanning from 10^{-3} to 1 mol L^{-1}). The examination of linear voltammograms has identified specific potential ranges for the sulphite oxidation process on the AISI 304 electrode in relation to sulphite content in the alkaline electrolyte. The anodic branches of the voltammetric plots exhibit substantial depolarisation at elevated sulphite concentrations (10^{-1}, 0.5, and 1 mol L^{-1}), signifying that sulphite undergoes oxidation via an electronation process occurring directly on the electrode. According to the existing theories it is indicated that the process transpires in a singular monoelectronic step, involving the intermediary production of dithionate species. Moreover, the charge transfer step governs the kinetics of the oxidation process at potential ranges where current densities are not limited by the diffusion of sulphite ions on the anode surface. Consequently, the anodic transfer coefficient α and the exchange current density i_o, which characterise the electrode process, may be determined.

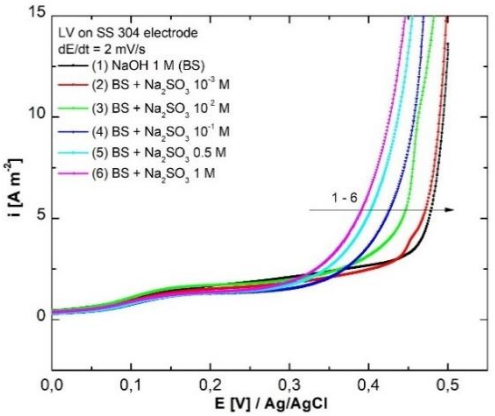

Fig. 2. Linear voltammograms recorded on the SS304 electrode at working concentrations, polarization rate 2 mV/s.

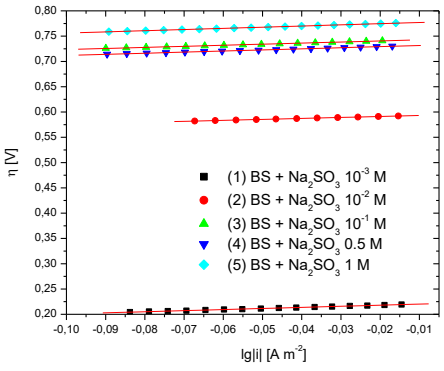

Fig. 3. Tafel slopes for sulfite oxidation on SS304 in alkaline test solutions.

Pseudo-potentiostatic conditions for the electrode processes were maintained by obtaining linear polarisation (Tafel) plots at a low polarisation scan rate of 1 mV s^{-1}. Table 1 presents the established kinetic parameters, whereas Figure 2 illustrates the associated Tafel plots for anodic polarisation. As expected, the voltametric profiles progressively transition to lower overpotentials with an increase in sulphite concentration in the alkaline solution. This demonstrates the enhanced kinetics of charge transfer at the electrode/electrolyte contact. The Tafel relationship shows how the charge transfer overpotential η depends on the net current density i for anodic processes. The intercept a and the slope b are defined as follows (Equations 6 and 7):

$$a = -\frac{2.303RT}{\boldsymbol{\alpha} zF} \lg i_o \tag{6}$$

$$b = \frac{2.303RT}{\boldsymbol{\alpha} zF} \tag{7}$$

where R is the universal gas constant (8.314 J mol^{-1} K^{-1}), T - thermodynamic temperature, K, F - Faraday constant (96,485 C mol^{-1}), z – number of transferred electrons.

Table 1 shows the values of α and i_0 that were found from Tafel plots. The values he found for the transfer coefficient α are between to 0.12–0.20, which supports a one-electron charge transfer process. The exchange current density i_0 values go up a lot as the concentration of sulphite goes up. At 0.1 mol L^{-1} Na_2SO_3, they reach above 411 A m^{-2}, which means that the charge transfer mechanism is quite quick. This means that the step that controls the rate of sulphite oxidation on AISI 304 is the direct transfer of electrons from the adsorbed sulphite to the electrode (9).

Table 1. Kinetic parameters of tested solutions

Na_2SO_3 conc [mol L^{-1}]	***b* [mV dec^{-1}]**	**α**	**i_o [A m^{-2}]**
10^{-3}	216	0.12	2.79
10^{-2}	232	0.11	28.43
10^{-1}	212	0.12	33.00
0.5	158	0.16	103.53
1	132	0.20	411.49

$$SO_3^{2-} \rightarrow {}^{\bullet}SO_3^{-} + e^- \tag{9}$$

In the possible range for the oxidation of SO_3^{2-} to SO_4^{2-}, it is conceivable that two things happen at the same time: direct oxidation and the creation of intermediate radical species. As a result, the kinetic parameters obtained should be considered apparent values, reflecting a composite mechanism rather than a simple one-step electron transfer.

3.3. Chronoamperometry

Chrono-electrochemical measurements had as a starting point the linear voltammograms shown in Figure 4. Analysing these curves, four potential steps were chosen (-0.25, 0.00, 0.25 and 0.50 V) to highlight the anodic processes that occur at electrode/electrolyte interface in tested system. From these values, the first three ones correspond to the sulphite oxidation plateau in alkaline solutions and the last one (0.50 V) is assigned to the oxygen evolution reaction (OER) simultaneously with the oxidation of the sulfite ions in the electrolyte, arising the possibility of a mixed process of chemical oxidation (with the participation of the atomic and molecular oxygen formed) – electrochemical of the sulfite ions on the interface or in the electrolyte adjacent to it.
In Figure 4 there are presented the results for sulphite oxidation during 60 minutes on working electrode in alkaline solutions with different sulphite ions concentrations at 0.00 V/Ag/AgCl.

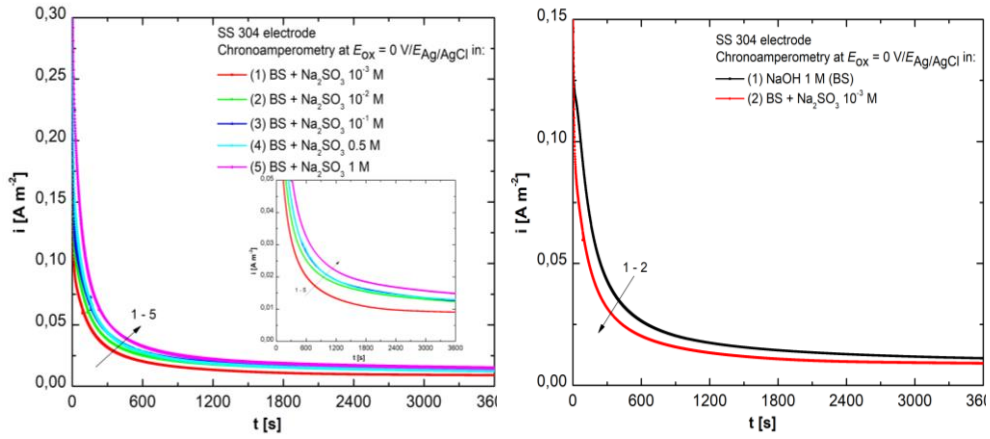

a) b)

Fig. 4. Current-time curves for AISI 304 electrode in 1 mol L-1 NaOH solution with different sulphite concentrations, at Eox= 0.00 V in al tested solution (a) and comparation between BS and 1 mol L-1 NaOH + 10-3 mol L-1 Na2SO3 solution (b).

Also, in Figure 4 there are presented the results for sulphite oxidation on AISI 304 in alkaline electrolyte with 10^{-1} mol L^{-1} Na_2SO_3 at all four potential values (a) and for E_{ox}= 0.00 V in 3 tested solution (10^{-1}, 0.5, 1 mol L^{-1} Na_2SO_3).
From the chronoamperometric data, we can deduce the following aspects:
- The potential range characteristic for the SO_3^{2-} oxidation process in alkaline solution is independent of the sulphite concentration in the electrolyte, situated between 0.00 and 0.25 V. Figure 5 illustrates that, for determinations performed at -0.25 V, cathode currents are observed after approximately 40 minutes;

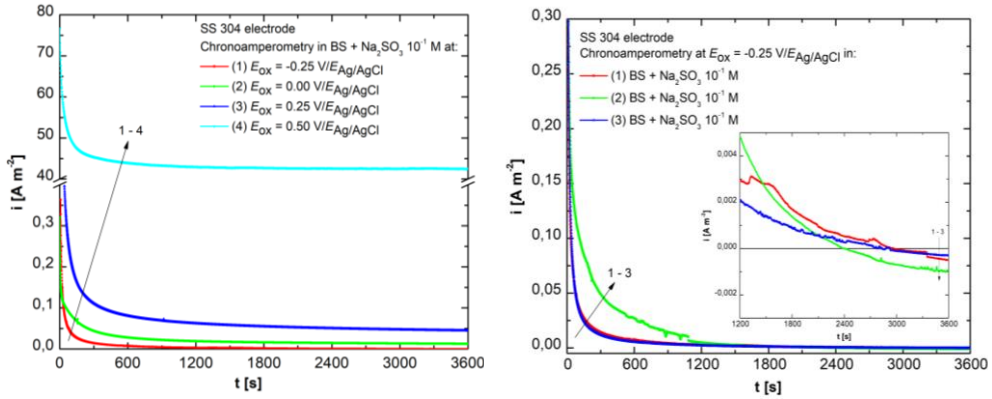

a) b)

Fig. 5. Current-time curves for AISI 304 electrode in 1 mol L-1 NaOH + 10-1 mol L-1 Na2SO3 solution solution with different sulphite concentrations (a) and comparation between three tested solution at same potential (- 0,25 V) (b).

- At elevated positive potential levels, the simultaneous oxidation of SO_3^{2-} and the oxygen evolution reaction (OER) transpires at the electrode/electrolyte interface, as evidenced by the characteristics and measurements of the current-time curve obtained at E_{ox} = +0.50 V;
- The current densities measured for all test solutions increase with the augmentation of sulphite concentration in the electrolyte.

By correlating these values with cyclic and linear voltammetric data, we can infer that the addition of sulphite in alkaline electrolyte enhances the first phase of the oxygen evolution reaction, as indicated by the change of the characteristic potential to higher negative values.

3.4. Electrochemical impedance spectroscopy

Based on cyclic and linear voltammograms, confirmed by chronoamperometric measurements, electrochemical impedance spectra were recorded on AISI 304 electrode in range of specific oxidation potential for sulphite ions added in alkaline test solutions. Also, for all concentration of Na_2SO_3, impedance measurements are conducted at 0.00 and 0.25 V/AgAgCl. The recorded results and fitted data are presented in the Nyquist complex plane representation in Figures 6 and 7. The Nyquist plots comprise two deformed semicircles. The initial semicircle represents the oxidation of the working electrode's surface, leading to the creation of an oxide layer upon which sulfite oxidation will occur. The surface is initially clean and treated before to each measurement; nevertheless, upon anodic polarisation of the electrode, oxidation processes of the constituent metals of stainless steel 304 occur at that level. The second semicircle, characterised by a bigger diameter, corresponds to the oxidation process of sulfite in an alkaline environment on the

working electrode.The graphical representation of the Nyquist dots confirms that both the oxidation of the electrode surface and the sulphite oxidation process are controlled by one charge transfer step. The experimental impedance data were fitted to the electrical equivalent circuit (EEC) presented in Figure 8, using a complex non-linear least squares (CNLS) procedure. The EEC consists in a solution resistance R_s which represents the uncompensated solution resistance, bound in series with two parallel connection (one for each electrochemical process carried out at the electrode-electrolyte interface opened above) between a constant phase element (*CPE*) and a charge transfer resistance R_{ct}.

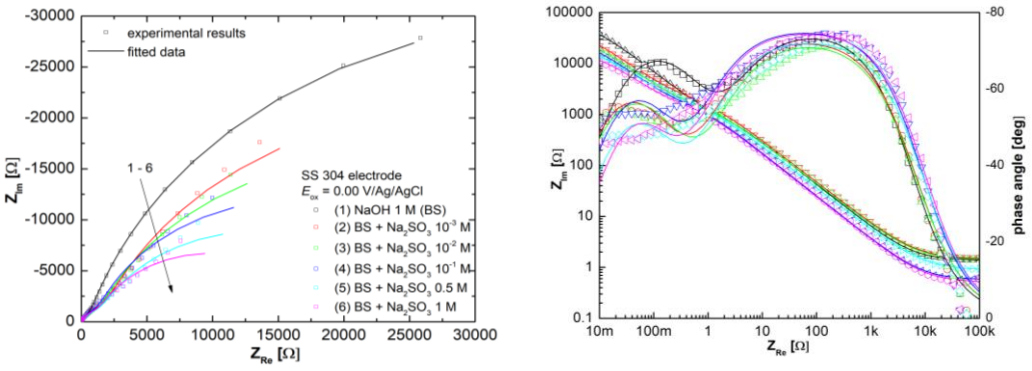

a) b)

Fig. 6. EIS spectra (Nyquist and Bode plots) for sulphite oxidation on AISI 304 electrode in 1 mol L-1 NaOH solution with different SO32- iones concentration at Eox = 0.00 V.

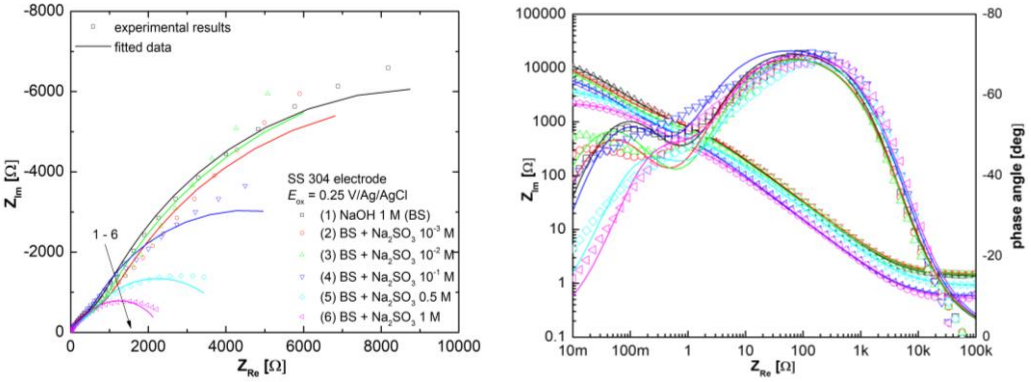

a) b)

Fig. 7. EIS spectra (Nyquist and Bode plots) for sulphite oxidation on AISI 304 electrode in 1 mol L-1 NaOH solution with different SO32- iones concentration at Eox = +0.25 V.

In the real electrochemical systems, CPE element characterized more precisely double layer capacity (C_{dl}) thus replacing the ideal capacitor (C). The obtained fitting results are shown as continuous line in graphical EIS data and the corresponding values of EEC elements are shown in Table 2.

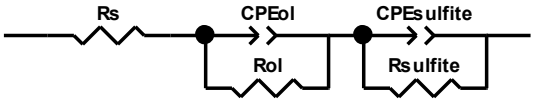

Fig. 8. Equivalent electrical circuit for modelling sulphite oxidation on AISI 304 electrode in alkaline solution.

Table 2. Calculated values of the circuit elements for modelling sulphite oxidation on AISI 304 electrode in alkaline solution

			AISI 304 surface oxidation			***Sulfite ions oxidation***				
Na_2SO_3 conc. [mol L^{-1}]	***E*** **[V]**	***R_s*** [Ω cm^2]	***T_1*** · **10^4** [F cm^{-2} s^{n-1}]	**n_1**	***$R1_{ct}$*** [Ω cm^2]	***T_2*** · **10^4** [F cm^{-2} s^{n-1}]	**N_2**	***$R2_{ct}$*** [Ω cm^2]	***C_{dl}*** · **10^5** [F cm^{-2}]	**Chi^2 · 10^3**
SB	0.00	1.37	1.94	0.84	527	2.15	0.84	75589	4.87	4.67
10^{-3}		1.46	1.51	0.83	1485	3.49	0.77	57306	4.36	6.71
10^{-2}		1.40	1.68	0.83	1057	4.01	0.78	45786	5.48	7.29
10^{-1}		0.57	1.77	0.84	1057	4.73	0.80	31201	6.42	2.49
0.5		0.88	1.90	0.85	1208	5.57	0.81	24398	9.86	2.13
1		0.51	2.55	0.86	1109	6.43	0.83	17537	12.1	2.85
SB	0.25	1.34	2.3	0.84	545	5.41	0.78	17127	7.40	5.71
10^{-3}		1.45	2.17	0.82	748	7.24	0.76	16638	8.46	7.36
10^{-2}		1.40	2.25	0.839	568	7.76	0.77	18681	9.84	7.73
10^{-1}		0.57	3.19	0.84	385	8.39	0.78	8354	9.62	2.26
0.5		0.89	4.13	0.84	328	8.99	0.79	3873	12.7	9.91
1		0.51	5.50	0.85	185	9.63	0.80	2152	14.1	2.44

Analysis of the results from Table 2 reveals that R_{ct} values markedly decline with increasing potential and sulphite content, indicating that sulphite electrooxidation occurs at an accelerated rate, corroborating the voltammetric data. The values for double layer capacitance (C_{dl}) have been computed. The double layer capacity increases with the rising polarisation. The buildup of a greater concentration of sulphite in solution near the electrode enhances the double layer capacitance.

3.5. Surface morphology

It has been used a confocal laser scanning microscope (Olympus LEXT OLS4000, 3D mode) to examine the surface topography and assess the morphological alterations of the particles during oxidation by sulfite in alkaline circumstances. Optical 3D profilometry enabled detailed examination of roughness, defects, and surface degradation at a micrometric scale. Following electrochemical assessments of the AISI 304 electrode surface in 1 mol L^{-1} NaOH with varying concentrations of Na_2SO_3, three representative regions were identified: (i) an unaltered area, (ii) a

transitional zone between the unaltered and corroded regions, and (iii) a severely corroded area.

It has been examined each region using both intensity mode and height map mode, and we additionally captured 2D optical micrographs to illustrate greater structural detail.The pristine surface has a finely polished form, as illustrated in Figures 9a–c. It features parallel mechanical abrasion lines and minimal topographical noise. The 3D height distribution (Figure 1b) indicates that the surface is predominantly flat, exhibits low roughness, and possesses a height range of under 130 μm.

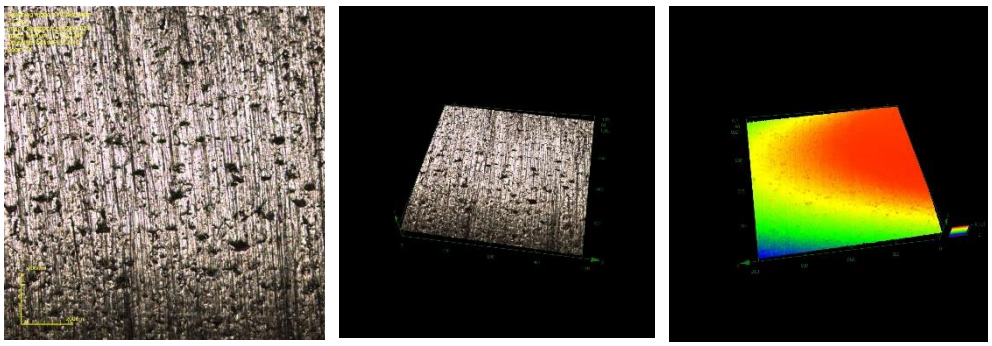

(a) (b) (c)

Fig. 9. (a) 2D optical micrograph, (b) 3D height map, and (c) combined 2D–3D visualization of the clean AISI 304 surface (reference zone) before electrochemical testing in NaOH + Na_2SO_3 solution.

Only a few minor pits remain, either resulting from the inherent imperfections of the original material or the processes employed to prepare the surface. In the transition zone (Figures 10a–c), the quantity and depth of surface imperfections significantly increase. The optical view reveals additional dark pits and fractured grooves that partially obscure the original polish markings. The accompanying 3D profile (Figure 10b) exhibits significant roughness and a height range of around 110 μm, indicating the onset of localised corrosion.

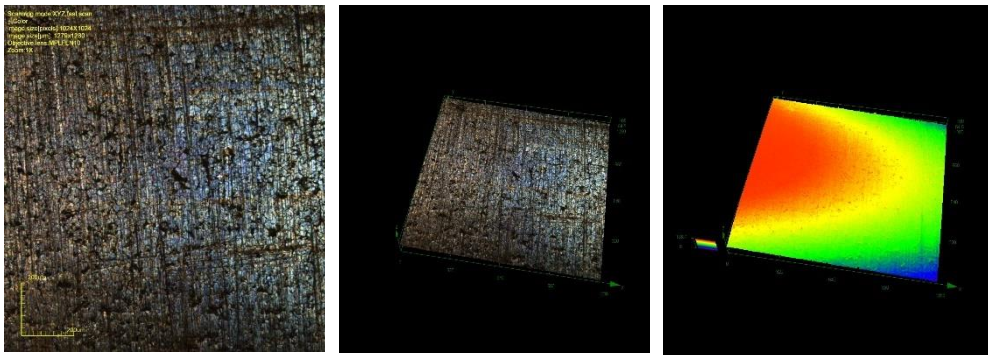

(a) (b) (c)

Fig. 10. (a) 2D optical micrograph, (b) 3D height map, and (c) 3D surface image of the transition zone between clean and corroded areas of the AISI 304 electrode.

The superficial depressions and textured micro-regions indicate that anodic oxidation processes influenced this area, albeit to a lesser extent than in the corroded zone. This configuration aligns with the intermediate behaviour observed in voltammetric curves at mid-range Na_2SO_3 concentrations (0.1–0.5 mol L^{-1}), where charge transfer accelerates while corrosion remains minimal. This region serves as a benchmark for assessing the topographical damage resulting from the electrochemical oxidation of SO_3^{2-} ions.

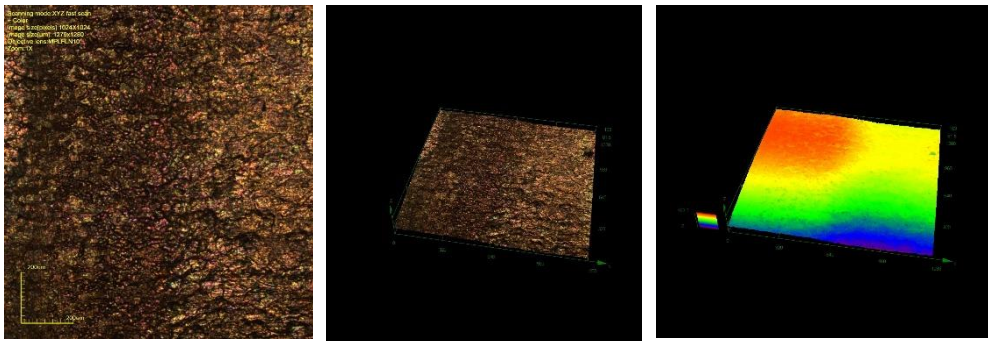

(a) (b) (c)

Fig. 11. (a) 2D optical image, (b) 3D height distribution, and (c) 3D textured view of the heavily corroded zone of the AISI 304 electrode.

The most impacted surface, illustrated in Figures 11a–c, exhibits numerous pits, profound disintegration craters, and a rugged texture that appears to be the result of an unintended process .The optical micrograph indicates that the surface is no longer smooth and has sustained significant damage. The 3D height map indicates significant topographical irregularity, with height values surpassing 160 μm. This configuration aligns with robust anodic oxidation processes at elevated sulphite concentrations (e.g., 1 mol L^{-1}), wherein the voltammetric curves exhibit diminished polarisation (refer to Figure 1), and the exchange current density and electron transfer accelerate. The alterations in surface morphology seen across the three zones correspond well with the electrochemical behaviour delineated in the linear voltammetry and Tafel analysis. The progressive deterioration of the surface indicates an increase in oxidation current density and an enhancement in the charge transfer mechanism as sulfite content increases.

4. Conclusions

The electrochemical oxidation of sulphite ions on AISI 304 electrodes in alkaline media was investigated using linear and cyclic voltammetry, potentiodynamic polarization (Tafel analysis), chronoamperometry, impedance spectroscopy (EIS), and three-dimensional surface morphology. Cyclic voltammetry provides additional evidence of preferred sulphite oxidation, demonstrating that sodium sulphite modifies the electrochemical profile of AISI 304 by diminishing the anodic oxygen peak at low concentrations and entirely raising it at high

concentrations. Decreased scan rates enhanced the resolution of oxidation processes, while anodic currents increased in accordance with the sulphite concentration. Anodic depolarisation and current densities increased with rising Na_2SO_3 concentration, as indicated by linear sweep voltammetry, implying a rapid, charge-transfer-controlled mechanism. Anodic transfer coefficients (α) varied between 0.12 and 0.20, while exchange current densities (i_0) exceeded 411 A m^{-2} at high sulphite concentrations, corroborating this behaviour through Tafel analysis. The potential range for sulphite oxidation (0.00–0.25 V) remains consistent across various concentrations, as indicated by chromatoamperometric findings. The oxidation of sulfite and the oxygen evolution process (OER) coincide at elevated positive potentials (+0.50 V). The current density increased with the rising concentration of sulphite, suggesting that sulphite facilitates the initial phase of the oxygen evolution reaction by shifting its beginning to higher negative potentials. The charge transfer resistance (R_{ct}) significantly decreased with rising voltage and sulfite concentration, signifying enhanced oxidation, as evidenced by EIS data that supported the voltammetric and chronoamperometric findings. Enhanced polarisation led to an augmentation in double-layer capacitance (C_{dl}), signifying increased ion accumulation at the interface. The electrochemical trends were corroborated by three-dimensional surface morphology. Localised surface deterioration at elevated sulfite concentrations was evidenced by the corroded area's profound pits and increased roughness in contrast to the unreacted surface's little roughness. In summary, sulphite ions expedite surface deterioration while concurrently facilitating rapid and efficient oxidation of AISI 304 in alkaline environments. The amalgamation of techniques confirms a charge-transfer-controlled, monoelectronic mechanism that influences electrode stability and kinetics, intensifying with concentration.

References

[1] https://www.google.com/search?client=firefox-b-e&q=Latimer+diagram+sulphur#vhid=vOg-UG4BojRPjM&vssid=l (accessed on 21.05.2025).

[2] Vaszilcsin N., Nemeş M., *Introduction to Electrochemistry*, Editura Politehnica, 2009.

[3] Fernández-García E., Merino P., González-Rodríguez N., Martínez L., Del Pozo M., Prieto J., Blanco E., Santoro G., Quintana C., Petit-Domínguez M. D., Casero E., Vázquez L., Martínez J. I., Martín-Gago J. A., *Enhanced Electrocatalysis on Copper Nanostructures: Role of the Oxidation State in Sulfite Oxidation*, ACS Catalysis, **14**, 15, 2024, p. 11522–11531.

[4] Cui B., Wang S., Guo X., Zhao Y., Rohani S., *An Integrated Electrochemical System for Synergistic Cathodic Nitrate Reduction and Anodic Sulfite Oxidation*, Molecules, **28**, 12, 2023, p. 4666.

[5] Skavas E., Hemmingsen T., *Kinetics and mechanism of sulphite oxidation on a rotating platinum disc electrode in an alkaline solution*, Electrochimica Acta, **52**, 2007, p. 3510–3517.

[6] Zelinsky A. G., *Features of Sulfite Oxidation on Gold Anode*, Electrochimica Acta, **188**, 2016, p. 727–733.

[7] Diaz-Abad S., Millan M., Rodrigo M. A., Lobato J., *Review of Anodic Catalysts for SO_2 Depolarized Electrolysis for "Green Hydrogen" Production*, Catalysts, **9**, 2019, p. 63.

[8] Enache A. F., Dan M. L., Vaszilcsin N., *Voltammetric Studies on Anodic Oxidation of Sulphite in Alkaline Solutions on Smooth Nickel-Based 3 Layers Platinum Nanoparticles Electrode*, Proceedings of the Georgian National Academy of Sciences, Chemical Series, **42**, 2016, p. 345–349.

[9] Enache A. F., Dan M. L., Vaszilcsin N., *Sulphite Electrooxidation in Alkaline Media on Skeletal Nickel-Based 6 Layers Platinum Nanoparticles Electrode*, Advanced Engineering Forum, **27**, 2018, p. 176–187.
[10] Kovaleva S. V., Aksinenko O. S., Korshunov A. V., *Electrooxidation of Sulfite Ions on a Composite Carbon-Containing Electrode Modified with Submicron Gold Particles*, Journal of Analytical Chemistry, **75**, 10, 2020, p. 1348–1357.
[11] Scott K., Cheng H., Taama W., *Zirconium and Ebonex as Cathodes for Sulphite Ion Oxidation in Sulphuric Acid*, Journal of Applied Electrochemistry, **29**, 1999, p. 1329–1338.
[12] Lăboșel M. A., et al., IOP Conference Series: Materials Science and Engineering, 1319, 2024, p. 012035.
[13] Domínguez-Jaimes L. P., Arenas Vara M. Á., Cedillo-González E. I., Ruiz Valdés J. J., De Damborenea J. J., Conde Del Campo A., Rodríguez-Varela F. J., Alonso-Lemus I. L., Hernández-López J. M., *Corrosion Resistance of Anodic Layers Grown on 304L Stainless Steel at Different Anodizing Times and Stirring Speeds*, Coatings, **9**, 2019, p. 706.
[14] Myung S. T., Sasaki Y., Saito T., Sun Y. K., Yashiro H., *Passivation Behavior of Type 304 Stainless Steel in a Non-Aqueous Alkyl Carbonate Solution Containing $LiPF_6$ Salt*, Electrochimica Acta, **54**, 24, 2009, p. 5804–5812.
[15] Lăboșel M. A., Duca D. A., Vaszilcsin N., Dan M. L., *Electrochemical Oxidation of Sulphite in Neutral Media on Graphite*, Materials Today: Proceedings, **45**, 5, 2021, p. 4233–4236.
[16] Khamme E., Sakdanuphab R., *Study of corrosion properties of carbon steel, 304 and 316L stainless steels in sulfuric acid and their degradation products*, Journal of Metals, Materials and Minerals, **33**, 4, 2023, p. 1672
[17] Corte L., Roscini L., Zadra C., Antonielli L., Tancini B., Magini A., Emiliani C., Cardinali G., *Effect of pH on potassium metabisulphite biocidic activity against yeast and human cell culture*, Food Chemistry, **134**, 2012, p. 1327–1336.